Table 1 Standard deviation of measurement errors

Specific force	A_z	0.012 m/s^2
Pitch rate	q	0.017 deg/s
Airspeed	V	0.150 m/s
Angle of attack	α	0.030 deg
Elevator deflection	δ_e	0.014 deg

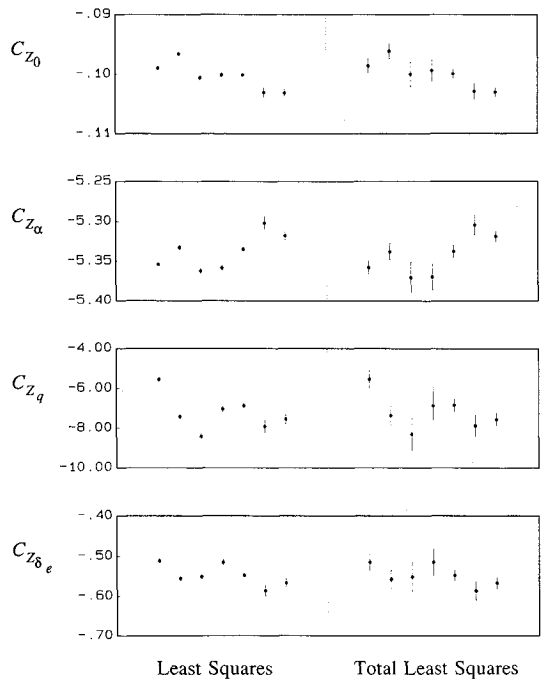

Fig. 2 LS/TLS estimation results C_Z equation. [Dot = estimated parameter value, Eqs. (3) and (10), and bar = predicted standard deviation, Eqs. (4) and (11).]

Parameter Identification Results

Data from 7 elevator doublets and 3211 flight test maneuvers were collected and analyzed with least squares and total least squares. The results are shown in Fig. 2.

The first column of Fig. 2 shows the least squares estimation results. The theoretical standard deviations were calculated according to Eq. (4) and seem to predict a high accuracy of the LS parameter estimates. However, it falls short in explaining the true scatter seen between the parameter estimates from the seven different maneuvers.

The second column of Fig. 2 shows the total least squares estimation results. The TLS parameter estimates do not differ significantly from the LS results, which is due to the high signal-to-noise ratio obtained with flight test instrumentation systems. Yet, Fig. 2 shows how the theoretical TLS standard deviations, calculated according to Eq. (11), differ significantly from the LS results. TLS accounts for all measurement error sources correctly (Table 1), while LS ignores errors on the explanatory variables and accounts for errors on C_Z only. This results in an incorrect overconfidence in the LS results. Notice that the TLS standard deviations agree better with the observed scatter between the results of different maneuvers.

Conclusions

TLS estimation was introduced in the field of aircraft parameter identification. Its merit is found in accurately accounting for multiple sources of (random) errors in a flight test instrumentation system. Unlike LS estimation, TLS was shown to give realistic predictions of the standard deviations of its estimates.

References

[1]Greenberg, H., "A Survey of Methods for Determining Stability Parameters of an Airplane from Dynamic Flight Measurements," NACA TN 2340, April 1951.

[2]Gerlach, O. H., "Determination of Performance, Stability and Control Characteristics from Measurements in Non-Steady Manoeuvres," AGARD-CP-17, Sept. 1966, pp. 499–523.

[3]Gauss, C. F., "Theoria Motus Corporum Coelestium in Sectionibus Solem Ambientium," Univ. of Göttingen, Germany, 1809.

[4]Golub, O. H., and Van Loan, C. F., "An Analysis of the Total Least Squares Problem," *SIAM Journal of Numerical Analysis*, Vol. 17, No. 6, 1980, pp. 883–893.

[5]Gleser, L. J., "Estimation in a Multivariate Errors in Variables Regression Model: Large Sample Results," *Annals of Statistics*, Vol. 9, No. 1, 1980, pp. 24–44.

[6]Huffel, S., "Analysis of the Total Least Squares Problem and Its Use in Parameter Estimation," PhD Dissertation, Leuven Univ., Leuven, Belgium, 1987.

Effect of Viscous Drag on Optimum Spanwise Lift Distribution

Kamran Rokhsaz*
Wichita State University, Wichita, Kansas 67208

Introduction

TRADITIONALLY, Prandtl's[1] lifting line theory has been used in classical aerodynamics to show that the optimum spanwise lift distribution is an elliptic one. This theory is based on the assumption that the entire lift is concentrated on a single line spanning the wing. The wake is assumed to be flat, and the local flow over the wing is taken to be chordwise only. Under these assumptions, elliptic lift distribution is shown to minimize the induced drag.

Numerical techniques such as vortex lattice methods have offered new approaches to optimization. These methods allow the user to manipulate the chordwise as well as the spanwise distribution of lift for minimum induced drag. Examples can be found in Refs. 2 and 3. In these methods, the induced drag due to lift is modeled in a variational form with lift as the constraint and the induced drag as the quantity to be extremeized. Another approach, based on a modified version of Multihopp's lifting surface theory can also be found in Ref. 4.

The general logic in all these cases has been that the viscous and induced drags can be optimized and then added directly. One of the flaws of this approach is that the spanwise lift distribution is based on circulation that is generated within the boundary layer. The same circulation (and therefore, the boundary layer) is also responsible for viscous drag. Therefore, the spanwise lift distribution that minimizes the induced drag may not necessarily minimize the viscous drag, and therefore, the total drag. Subsequently, it is the intention of this note to show how Prandtl's method can be modified to account for viscous drag. It will be demonstrated that the inclusion of the viscous drag renders the elliptic lift distribution nonoptimal. It will also be shown that elliptic lift distribution, although nonoptimal, is quite close to the optimum case.

Method of Analysis

The development presented here very closely follows those of standard texts in aerodynamic theory, such as Refs. 5 and

Received Nov. 4, 1991; presented as Paper 92-0287 at AIAA 30th Aerospace Sciences Meeting, Reno, NV, Jan. 6–9, 1992; revision received March 8, 1992; accepted for publication March 20, 1992.

*Assistant Professor of Aerospace Engineering, Department of Aerospace Engineering. Senior Member AIAA.

6. In general, the spanwise lift distribution is assumed to be concentrated on the lift line extending from wing tip to wing tip. Along this line, the distribution of circulation is represented by a Fourier series of the form

$$\frac{2\Gamma(y)}{CV_\infty} = 2\pi \sum_{n=1}^{\infty} A_n \sin(n\theta) \tag{1}$$

where

$$\theta = \cos^{-1}(-2y/b) \tag{2}$$

Direct integration can show

$$C_L = C_1 A_1 \tag{3}$$

$$C_{D_i} = C_2 \sum_{n=1}^{\infty} nA_n^2 \tag{4}$$

where minimum induced drag is obtained if

$$A_1 \neq 0 \quad \text{and} \quad A_2 = A_3 = \cdots = 0 \tag{5}$$

This, then according to Eq. (1), results in elliptic distribution of lift across the span.

Throughout this development the flow is assumed to be chordwise. Thus, the contribution of viscous drag can also be added at this point. For the sake of simplicity, let the viscous drag coefficient of the airfoil vary quadratically with local lift coefficient. This implies then that the local viscous drag coefficient can be expressed as a quadratic function of the local circulation, or

$$c_{d_v} = f(\Gamma^2) = a_1 + a_2(2\Gamma/CV_\infty)^2 \tag{6}$$

Integrating this over the wing span and regrouping the constants results in

$$C_{D_v} = C_4 + C_3 \int_0^\pi \sum_{n=1}^{\infty} A_n \sin(n\theta) \sum_{k=1}^{\infty} A_k \sin(k\theta)\sin(\theta)\, d\theta \tag{7}$$

This integral results in

$$C_{D_v} = C_4 + C_3 \sum_{n=1}^{\infty} \sum_{k=1}^{\infty} A_n A_k \cdot \left[\frac{1}{1-(n-k)^2} - \frac{1}{1-(n+k)^2}\right] \tag{8}$$

where the integers n and k in this expression are odd only. The value of A_1 is determined from the lift coefficient. Now for optimum the spanwise lift distribution, the remaining Fourier coefficients have to be found such as to minimize the sum of the induced and viscous drags. Without the contribution of the viscous drag, all these coefficients with the exception of the leading one had to be zero. Inclusion of viscous drag nullifies this requirement, resulting in a nonelliptic spanwise lift distribution.

Results and Discussion

As a test case, a rectangular wing of aspect ratio of six was considered. The airfoil was assumed to be thin and symmetric with lift curve slope of 2π/rad. The Fourier series was truncated at six terms, resulting in three nonzero coefficients. The following model was used for viscous drag coefficient:

$$c_{d_v} = 0.0058 + 0.0064c_l^2 = 0.0058 + 0.0064(2\Gamma/CV_\infty)^2 \tag{9}$$

This model approximately represents the NACA-0012 airfoil at Reynolds number of three million as given in Ref 7. Figure 1 shows the comparison of the experimental data and this model for this airfoil. References 5 and 6 show that for this type of planform

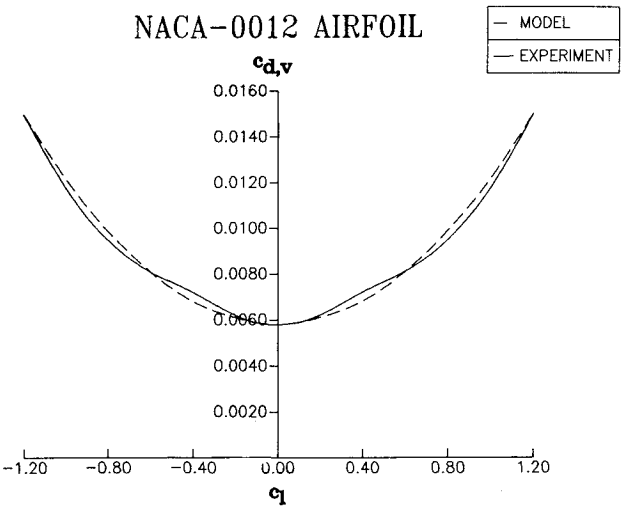

Fig. 1 Comparison of the experimental and the modeled airfoil viscous drag coefficients.

Table 1 Comparison of induced and viscous drags

Optimum			
Lift coeff. coefficient	Induced drag coefficient	Viscous drag coefficient	Total drag coefficient
0.25	0.00332	0.00623	0.00955
0.50	0.01327	0.00752	0.02079
0.75	0.02985	0.00968	0.03953
1.00	0.05306	0.01269	0.06575
Elliptic			
Lift coeff. coefficient	Induced drag coefficient	Viscous drag coefficient	Total drag coefficient
0.25	0.00332	0.00623	0.00955
0.50	0.01326	0.00753	0.02079
0.75	0.02984	0.00969	0.03953
1.00	0.05305	0.01272	0.06577

$$C_1 = (\pi^2/2) = 4.93480 \tag{10}$$

$$C_2 = (\pi^3/4\bar{A}R) = 1.29193 \tag{11}$$

$$C_3 = 2\pi a_2 = 0.12633 \tag{12}$$

$$C_4 = a_1 = 0.0058 \tag{13}$$

Equations (4) and (8) were added for total drag coefficient. To minimize the sum, the resulting expression was differentiated with respect to each Fourier coefficient and set to zero. This resulted in a set of linearly independent equations yielding the coefficients for optimum total drag. This process for the above airfoil and the wing resulted in

$$A_3 = 0.00842A_1 \quad \text{and} \quad A_5 = 0.00078A_1 \tag{14}$$

On the one hand, the above results clearly show that the optimum spanwise lift distribution differs from elliptic. On the other hand, judging from the magnitudes of the resulting Fourier coefficients, the optimum lift distribution is not very different from elliptic. The same argument also holds for the twist distribution corresponding to each case. The drag coefficients, both for elliptic and for optimum case, are presented in Table 1. This table shows the induced drag of the optimum case is indeed larger than that of the elliptic case. However, the difference in total drag between the two cases is quite small.

Table 2 Convergence of the Fourier series

Order of the series	6	10	20
A_3/A_1	8.418E−03	8.418E−03	8.418E−03
A_5/A_1	7.818E−04	7.831E−04	7.831E−04
A_7/A_1	—	1.853E−04	1.853E−04
A_9/A_1	—	6.516E−05	6.528E−05
A_{11}/A_1	—	—	2.870E−05
A_{13}/A_1	—	—	1.455E−05
A_{15}/A_1	—	—	8.149E−06
A_{17}/A_1	—	—	4.916E−06
A_{19}/A_1	—	—	3.136E−06

Table 3 Effect of aspect ratio on the optimum drag

Aspect ratio	Total drag coefficient (elliptic)	Total drag coefficient (optimum)
5	0.07638	0.07637
10	0.04455	0.04453
15	0.03394	0.03391
20	0.02863	0.02860
25	0.02545	0.02540
30	0.02333	0.02327

In the above example, a total of six terms was used in the Fourier series. Table 2 shows the convergence rate of the series for larger number of terms. It is quite evident from this table that the resulting series converges quite rapidly. The drag coefficients corresponding to the different cases presented in this table were identical.

The above example employed a wing with an aspect ratio of 6. As the aspect ratio changes, so would the relative significance of the induced drag and the viscous drag. Therefore, the problem was solved over a range of aspect ratios. The results are shown in Table 3. As expected, increasing the aspect ratio decreases the induced drag, increasing the significance of the viscous drag. This suggests that for high aspect ratio wings such as those on sail planes, the twist should perhaps be optimized for least total drag.

In all of the above cases, judging from the magnitude of the numbers, optimization for viscous drag does not appear to pay off. In every case, any reduction in viscous drag was nearly offset by a corresponding increase in induced drag. Even for large aspect ratio cases, where the induced drag tends to lose its dominance, the same gain in total drag can be realized by slightly increasing the aspect ratio. Furthermore, it is quite evident, that the base drag [i.e., 0.0058 in Eq. (9)] is the dominant part of viscous drag. So any effort in reducing the viscous drag should be concentrated on reducing this value.

Conclusions

It was demonstrated how the classical lifting line theory can be modified for the effect of viscous drag. The governing equations were developed and applied to a rectangular wing. The airfoil chosen for this example resembled NACA-0012 at Reynolds number of three million. Rapid convergence of the resulting series was demonstrated. It was shown that the inclusion of viscous drag indeed renders the elliptic lift distribution nonoptimal. However, in every case, the reduction in viscous drag was very closely matched by an increase in induced drag. Therefore, the reduction in total drag, within the confines of this theory, was determined to be negligible. Nonetheless, this exercise raises the possibility of employing similar techniques in conjunction with vortex lattice or panel methods.

References

[1]Prandtl, L, *Applied Hydro and Aeromechanics*, McGraw-Hill, New York, 1957.

[2]Loth, J. L, and Boyle, R. E., "Optimum Loading on Nonplanar Wings at Minimum Induced Drag," NASA Rept. AD-704502, Aug. 1969.

[3]Lundry, J. L., "A Numerical Solution for the Minimum Induced Drag, and Corresponding Loading, of Nonplanar Wings," NASA CR-1218, Nov. 1968.

[4]Lamar, J. E., "A Modified Multhopp Approach for Predicting Lifting Pressures and Camber Shape for Composite Planforms in Subsonic Flow," NASA TN-D-4427, July 1968.

[5]Moran, J., *An Introduction to Theoretical and Computational Aerodynamics*, Wiley, New York, 1984.

[6]Kuethe, A. M., and Chow, C.-Y., *Foundations of Aerodynamics*, 3rd ed., Wiley, New York, 1976.

[7]Abbott, I. H., and von Doenhoff, A. E., *Theory of Wing Sections*, Dover, New York, 1959.

PAN AIR Analysis of Simply Connected Control Surface Deflections

Seth A. Moyer*
Naval Air Warfare Center,
Warminster, Pennsylvania 18974

Nomenclature

FS, WL, BL = aircraft fuselage station, waterline, buttline, in.
M_∞ = freestream Mach number
n = upper surface unit normal
W = total mass flux
α, A = aircraft angle of attack, deg
α_{xz}, α_{xy} = local flowfield angle of upwash and sidewash, deg
β = nondimensional mass flux magnitude
Θ = flap deflection angle, deg positive down

Introduction

SEVERAL existing and planned fighter/attack aircraft have control surface deflection schedules that are dependent upon flight condition. Effective flowfield analysis of these aircraft must include proper modeling of leading- and trailing-edge flap effects. This is particularly important in store carriage and release analysis where a store is oriented such that there is significant interaction between the flap and store surfaces.

The present study analyzes PAN AIR flap modeling of simply connected control surfaces. Simply connected control surfaces are those surfaces that move with pure rotation, or systems that approximate pure rotation. A modeling method based on proper specification of the boundary condition, as suggested in Ref. 2, is compared to several geometric approaches based on previous studies of more complex configurations. It is demonstrated that the representation of simply connected flap deflections by boundary condition specification is both accurate and efficient.

Background

PAN AIR[1-4] has proven useful in the past for predicting the aircraft-induced flowfield for complex aircraft configurations where flap deflections are not present.[5,6] Several studies have also been conducted on flap configurations using various "exact" approaches for modeling the deflections with PAN AIR.[7] These studies have been centered on complex

Received Feb. 12, 1992; revision received March 23, 1992; accepted for publication March 26, 1992. This paper is declared a work of the U.S. Government and is not subject to copyright protection in the United States.

*Aerospace Engineer, Aircraft Division. Member AIAA.